Large-area solar irradiance mapping

Irradiance mapping | As PV systems proliferate, it is increasingly important to forecast their energy output in order to ensure a safe and reliable integration of their variable output into electric power grids. Dazhi Yang, André Nobre, Rupesh Baker and Thomas Reindl of SERIS outline a technique for generating large-scale 2D irradiance using data from pyranometers and plane of array reference cells

There are two main reasons for the development of accurate solar irradiance mapping, namely to calculate the so-called 'performance ratio' (PR, in %), and to use it as a critical input to perform solar irradiance forecasting. Many owners of PV systems do not know how well their installations perform because they have no on-site readings from an irradiance measurement device. They would only be able to gauge the quality of the systems if they had at least a close estimation of the irradiance values at their respective locations, which would then enable them to calculate PRs. The sheer solar energy generated over time, even if it is related to the installed capacity (so-called 'specific yield' in kilowatt hour per kilowatt peak – kWh/kWp), is not sufficient for judging the performance, since the baseline reference is missing and the output also fluctuates because of the year-on-year variability of the irradiance (there are 'good' and 'bad' solar years). So without the on-site irradiance, the PV system owner would not know whether the system 'could do better' or if the PV modules were possibly degrading faster than what had been guaranteed by the PV module manufacturer, for example.

Power system operators are often worried about the possible impact of the variability of energy generated from the increasing share of solar PV systems on the stability and resilience of the electric power grid. The solar power generation from PV modules naturally fluctuates with the available irradiance at the site, which is influenced by clouds and the absorbing or scattering constituents of the atmosphere. In order to support the power system operations, the ability to forecast the output of the PV systems would be helpful, probably not to the extent of advanced bidding as required from conventional power generators, but at least in terms of having a reasonable estimation of the solar power output over the next 15–30 minutes (typical dispatch cycles), intra-day (for ramping up or down of conventional capacities) or day-ahead (for futures trading). 'Reasonable' in that sense strongly depends on the climatic conditions and the forecasting horizon, but could go as low as less than 10% uncertainty. Forecasts (even long term) with greater than 50% accuracy are most probably not meaningful anymore.

Both the above-mentioned challenges could be addressed if (together with other techniques) there were a constantly updated, area-wide mapping of the solar resource available. Ideally, such a map is based on a dense network of irradiance sensors, but is restricted in many cases by the cost of high-precision pyranometers, real-time monitoring and frequent maintenance. However, many PV systems are in fact equipped with reference cells which are typically installed in the plane of array (POA) of the PV modules for evaluating and monitoring the performance of the PV system. Adding this network of reference cells to existing pyranometer networks (from meteorological services or research institutes) would allow the generation of large-area irradiance maps with improved resolution, which could then be used either to evaluate the performance of PV systems without an on-site irradiance reading capability, or to have a base for irradiance and solar power output forecasting for the grid operator. Since POA readings cannot be added to horizontal irradiance sensor data, this paper describes an irradiance conversion technique which allows POA irradiance measurements from an on-site reference cell to be converted to global horizontal irradiance (GHI). The converted GHI from each location can then be used for maps through spatial interpolation techniques, such as kriging – an interpolation technique which uses the spatial covariance to generate weightings.

Why and how to assess the performance of solar PV systems?

The performance of a PV system is usually assessed via two metrics: 1) the specific yield in kWh/kWp over a certain period of time (typically one year); and 2) the PR in %, which is a measure of how well a PV system converts the incoming solar flux into electricity, based on a) the amount of the solar resource reaching the POA of the PV installation, and b) the nominal system capacity at standard test conditions (STC). The latter measure gives the ratio of the actual AC energy yield to the 'theoretical' maximum DC yield, based on in-plane irradiance measurements and on the assumption of full DC-to-AC conversion.

Relatively independent of the irradiance on site, the PR is an internationally recognised metric for PV system performance assessment and is used for system evaluation all around the world. It has been adopted by the International Energy Agency (IEA) Photovoltaic Power Systems (PVPS) programme and is described in the IEC standard 61724 (1998).

'The performance ratio is an internationally recognised metric for PV system performance assessment and is used for system evaluation all around the world'

In order to measure the irradiance, silicon-wafer-based reference cells ('silicon sensors') are normally used in PV system installations, while pyranometers or calibrated silicon sensors are commonly used for research-grade investigations (see Fig. 1). It should be pointed out that the irradiance readings from a calibrated pyranometer (used for solar radiometric measurement, see below) are ~3–4% higher than those obtained using reference cells (due to the fact that pyranometers absorb a larger fraction of the solar spectrum), which in consequence results in a lower PR. In a later section, some of the loss mechanisms (the deviations of the reference cell measurements from the pyranometer measurements) will be discussed in detail. These deviations, however, are well known and can be accounted for in the conversion of POA readings to GHI to enable the generation of large-area irradiance maps from a network of multiple measurements devices.

Fig. 2 shows the performance ratio of 11

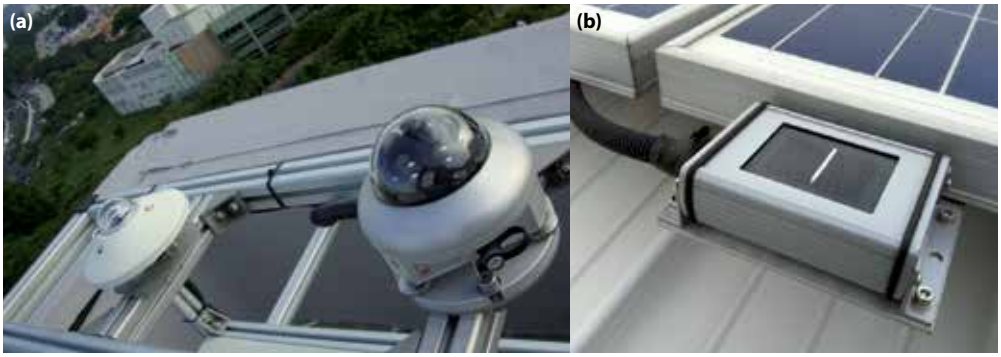

Figure 1. (a) Two pyranometers: a CMP11 from Kipp & Zonen (left), and an SPN1 from Delta-T (right); (b) a silicon sensor installed in the plane of array of a PV system.

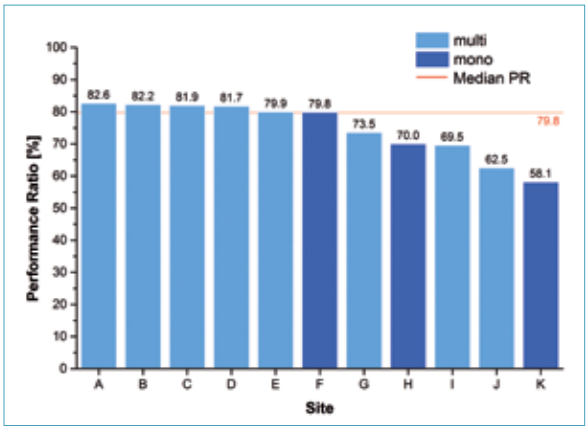

Figure 2. Measured PR of 11 silicon-wafer-based PV systems in tropical Singapore. The median performance value for the year 2011 was ~80%. (See Nobre et al. [1].)

silicon wafer-based PV systems in Singapore, assessed during 2011. PV systems in hotter climates will generally display a lower performance than in temperate climates.

Why and how to forecast solar irradiance?

Power system operation centres need to concurrently manage grid parameters (voltage, frequency, etc.), load flow, unit commitment, transient stability and transmission. A common goal of these operations is to meet the changing electricity demand and to minimise outages. Although highly complex, power system operation is well developed for conventional power generation, transmission and distribution. With the increasing penetration of distributed solar power into the electricity grids, the inherently introduced variability (i.e. from different irradiance levels because of cloud movements) potentially poses challenges for the power system operations. Despite there also being positive impacts on the power grid – such as the reduction of peak demand (especially in countries where the air conditioning load pattern matches the irradiance curve of the day) or reduced voltage drops in the distribution grid – the high ramp rates and sudden drops when clouds move over a PV installation are still seen as a threat by many grid operators. Apart from the more conventional approach of increasing the spinning reserves in the power system (which is a rather costly option), there are various other ways of managing this variability, some of which are:

- Suitable regulations for active and passive inverter reaction.
- Demand-side management (DSM) – advance notice in the range of hours.
- Direct load control – an extreme form of DSM for short notice periods (minutes).
- Energy storage – e.g. battery based, with instant reaction.

Complementary to the above-mentioned options, the forecasting of the solar power output on different timescales for a certain area is a very powerful tool, which brings solar PV one step closer to being 'dispatchable', and thereby making it more compatible with the current power grid operation. Solar energy forecasting is also compliant with future smart grids, where various devices and communication gateways can make automated decisions with respect to energy flows (e.g. self-consumption) and economic considerations (e.g. selling to the grid at peak demand).

Among various timescales of solar energy forecasting, medium-term forecasting (15 minutes to one hour, depending on the local dispatch cycle) is particularly important, especially with regard to the operations of peaking and load-following power plants. However, these forecast models are less developed than long-term and very short-term forecasts.

For long-term (several hours to a few days) solar irradiance forecasts, satellite-based techniques are commonly adopted [2]. The forecasts are usually derived from the output of so-called 'numerical weather prediction' (NWP) models; model output statistics are then used to post-process the forecasts. Depending on the location on the Earth, cloud motion analyses can be added in order to capture and project the dynamics of the clouds, from which the irradiance maps are then derived through a projection of the sky conditions. These prediction model methods can be traced back to the 1920s (when NWP was first proposed).

Very short-term (a few seconds to five minutes) irradiance forecasts can be separated into two classes of methods – one based on sky cameras and the other using high-spatial-resolution (a few metres apart) irradiance sensor networks. Both methods aim to provide a better understanding of cloud movements. Unlike NWP, these methods analyse cloud motion under local sky conditions. As the cloud motion is considered to be persistent within a small time window, these forecasts can accurately account for the up-and-down ramps in PV output [3].

Medium-term forecasting is a much more challenging problem, with no dominant strategies being available at the moment. Currently, spatio-temporal statistical models (such as time-forward kriging [4]), which use multiple irradiance sensors, or purely temporal statistical models [5], which use only one sensor, are usually adopted. In view of the effects of cloud propagation [6], spatio-temporal models are preferred over purely temporal models, which seek to identify the relationship between the points of forecast and past observations. In other words, past values are combined, either linearly or non-linearly, to form the forecasts through a regressive framework. In a spatio-temporal model, the past values from a particular station and from its neighbouring stations are used [7]. Space–time kriging and vector autoregressive models are examples of such spatio-temporal statistical models [8]. A common pre-requisite for applying these statistical models is a network of horizontally installed irradiance sensors, which measure the spatio-temporal irradiance distribution. Using the satellite-derived irradiance data for these statistical models may also be considered; however, satellite-derived irradiance usually has a higher uncertainty of ~8–25%. Moreover, it has low temporal resolution (typically 30 minutes to one hour) and low spatial resolution (1km to 10km), which may not capture the fast-changing irradiance random field. From a sampling point of view, a high spatial resolution of irradiance sensors is always desirable.

Irradiance measuring instruments

There are several accepted terms describing irradiance components (measured in W/m^2) used in modelling. Global horizontal

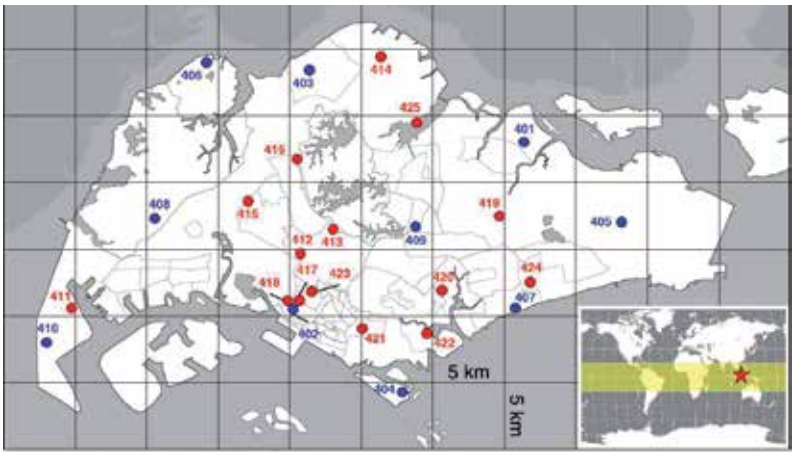

Figure 3. A network of 25 ground-based irradiance measurement stations in Singapore. The blue dots represent stations where both silicon reference cells and pyranometers are deployed. The red dots are stations where only reference cells are installed. The bottom right corner shows Singapore's position (red star) on the world map, as well as the 'sunbelt' region (yellow band) between the tropics of Cancer and Capricorn.

irradiance (GHI) refers to irradiance measured on a horizontal surface. It can be decomposed additively into two components: the horizontal beam irradiance (HBI), i.e. the beam irradiance on a horizontal plane; and the diffuse horizontal irradiance (DHI). On a tilted surface, tilted global irradiance (TGI) can be decomposed additively into the tilted beam irradiance (TBI), the tilted diffuse irradiance (TDI) and the reflected irradiance (RI). Theoretically, if any two (out of seven) types of irradiance listed above are known, the others can be 'deterministically' calculated through transposition models (see details below).

To measure the above-mentioned irradiance, two types of device – namely thermopile-based instruments and PV reference cells – are used. Pyranometers and pyrheliometers are thermopile-based instruments that convert heat to an electrical signal which can then be recorded. A pyranometer is typically used to measure GHI; if equipped with an additional shadow band to block the direct irradiance, it can also record DHI. Pyranometers are often installed in larger PV systems to also measure TGI (and possibly TDI), but in this case need to be installed in the tilted module plane. However, each pyranometer only records one of the irradiance components mentioned above.

A pyrheliometer measures the beam irradiance with a solar tracking system that aims the instrument at the sun. HBI and TBI can then be calculated using the zenith angle and the incidence angle respectively. Pyranometers and pyrheliometers are often used for solar radiometric measurements [9]. The price range of industrial-grade pyranometers can reach a few thousand US dollars.

The alternative reference cell is a PV device, which converts a flux of photons directly into an electric current using an external circuit, working similarly to a PV system. Most reference cells are silicon wafer based; they are less accurate than thermopile-based devices (the major loss mechanisms are discussed below). Hundreds of reference cell types are available on the market and are cheaper than pyranometers (a few hundred US dollars). This type of sensor is therefore often used to measure the POA irradiance at a PV site in order to assess the system performance [9]. A more detailed comparison of these instruments can be found in Meydbray, Emery & Kurtz [9].

In solar irradiance forecasting, solar radiometric measurements are preferred: hence high-precision pyranometers are typically used for this application [5]. Many research institutes – such as the Solar Energy Research Institute of Singapore (SERIS) – have taken the initiative to build irradiance measurement networks using pyranometers and/or reference cell devices [7,8]. Such an example is given in Fig. 3, which shows an irradiance network deployed in Singapore by SERIS.

'Once the loss mechanism issues are addressed, the reference cell can be used to approximate a solar radiometric measurement device'

In comparison to most networks currently available in the world, the network shown in Fig. 3 is rich in both temporal and spatial resolution for metropolitan-scale applications. Research has shown that the irradiance random process is extremely volatile [8]; a typical de-correlation distance of 1–10km is observed in many places of the world (a de-correlation distance is defined as the geographical distance over which cross-correlation between two irradiance time series is not observed anymore or is statistically insignificant). It should be noted that the de-correlation distance is a function of sampling frequency: a higher frequency corresponds to a smaller distance. With such considerations, an even denser network of irradiance sensors than the existing one described above would be desirable when the medium-term forecasts are performed at, for example, 15-minute intervals for grid utility management.

Should reference cells be used for radiometric measurements?

As mentioned earlier, reference cells are typically used for PV efficiency and performance measurements. When they are used in solar radiometric measurements, three issues need to be addressed.

The temperature response of the silicon reference cells is similar to that of a PV system, but needs to be adjusted in order to obtain accurate solar radiometric measurements. Although the temperature coefficient is a function of irradiance and temperature, it is typically assumed to be linear with respect to temperature [10]. Some of these reference cells possess an on-board temperature sensor that provides real-time temperature measurements, enabling irradiance readings to be corrected (either at the sensor output level, or via post-processing in the data acquisition system). To optimise their performance, such reference cells need to be calibrated. The Fraunhofer Institute for Solar Energy Systems (Fraunhofer ISE), along with other leading solar research institutes, provides such calibration services, thereby reducing the uncertainty of reference cells to as low as 2% under indoor testing conditions.

Furthermore, reference cells have a narrower wavelength response than pyranometers. This is straightforward to deal with, as the spectral loss is considered to be linear with irradiance. The spectral loss is compensated during post-processing after the measurements are obtained.

The third loss mechanism is the reflectance loss. As the response to the angle of incidence falls off at angles greater than 80°, this loss can be regarded as a function

Tilt	MBE [W/m²]	RMSE [%]	U95 [%]
10°	2.09	2.63	5.07
20°	–5.12	3.00	6.47
30°	–1.70	4.10	8.17
40°	–6.40	4.86	9.90

Table 1. Horizontal-to-tilt irradiance conversion errors using the Perez transposition model. The calculated TGI is compared with the actual TGI measured by reference cells tilted at four different angles. Mean bias error (MBE), root mean square error (RMSE) and the 95% expanded uncertainty (U95) are used as error metrics. All error terms include temperature, spectral loss and reflectance loss corrections.

of incidence angle. The compensation for the reflectance loss is performed at various bands of incidence angle using linear regression, i.e. for each band:

$$\textit{Reflectance loss} = a + b \times \textit{angle of incidence} \quad (1)$$

where a and b can be determined empirically.

Once the loss mechanism issues are addressed, the reference cell can be used to approximate a solar radiometric measurement device. The remaining challenge is to convert the tilted reference cell measurements to horizontal so that they can be integrated in spatio-temporal irradiance maps.

Conversion from tilt to horizontal using two reference cells

Transposition is used to calculate TGI based on actual GHI and DHI measurements. There are two types of transposition models: isotropic and anisotropic. The isotropic transposition model does not include the azimuthal dependency of the DHI; in other words, the diffuse component is assumed to be homogeneous in all directions. However, in reality, the diffuse component is affected by two main anisotropic mechanisms – the circumsolar and horizon brightening effects. Both mechanisms are due to the scattering of solar radiation by aerosols in the atmosphere. For these reasons, anisotropic transposition models are proposed in order to account for such characteristics.

Among various scientific models, the Perez transposition model [11,12] is considered to be a very reliable and universal model. It separates the sky hemisphere into three parts: an isotropic background, the circumsolar disk and a band near the horizon. The circumsolar disk and the horizon band contributions can be expressed as fractions of the diffuse background radiation. These coefficients are determined empirically using irradiance measurements from a selection of geographical locations, mostly in the USA. The performance of the Perez model has been validated numerous times in the literature and can be considered to be robust, even for regions outside of the original training pool.

▼Figure 4. The irradiance measurement station located on the roof at the Solar Energy Research Institute of Singapore (SERIS).

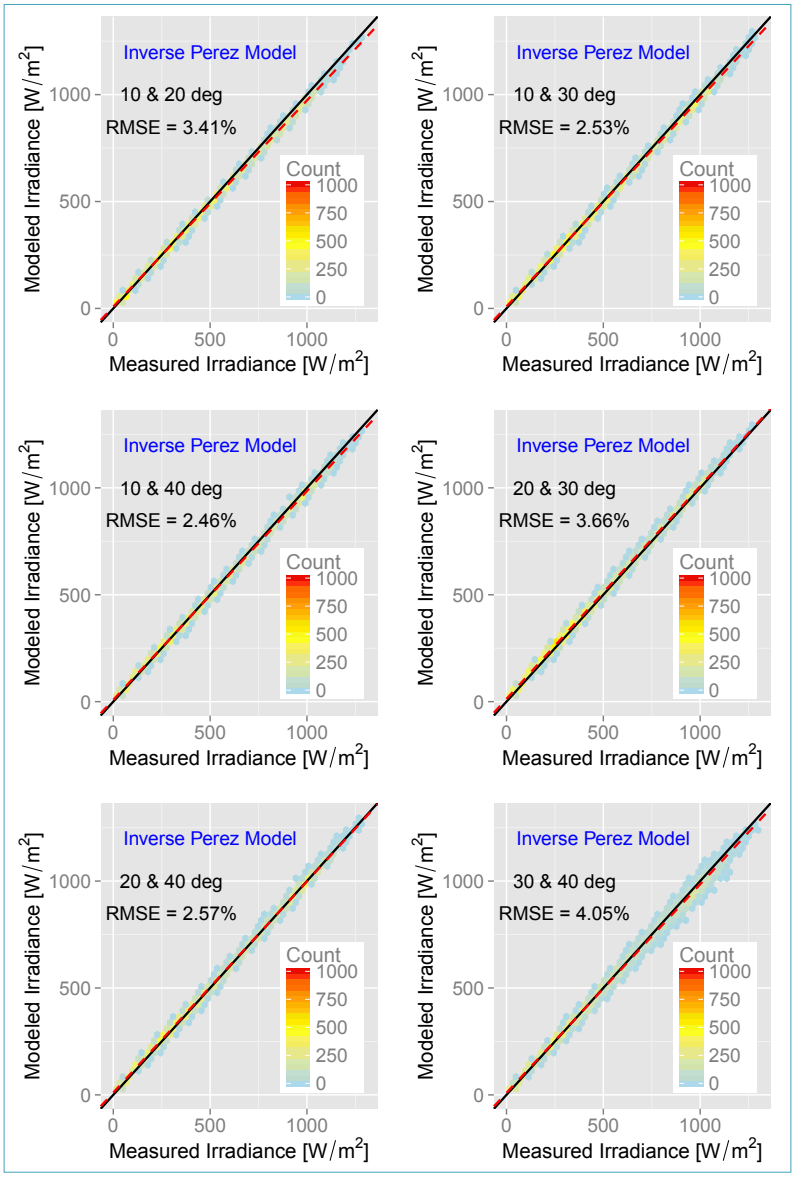

►Figure 5. Scatter plots of the 'inverse Perez model' using various combinations of reference cells. A hexagon binning algorithm is used for visualisation. The black solid lines are the identity lines, while the red dashed lines are the linear regression lines on the scatters.

Table 1 shows the Perez model errors for various test cases that have been conducted for Singapore. In this experiment, four tilted silicon reference cells from Mencke & Tegtmeyer (±5% uncertainty) were installed at 10°, 20°, 30° and 40° respectively, with a common azimuth angle of 64° NE (see Fig. 4). A Kipp & Zonen CMP11 pyranometer (±3% uncertainty) was installed horizontally. In addition, a SPN1 sunshine pyranometer (±5% uncertainty) from Delta-T Devices measured the diffuse horizontal irradiance. The horizontal irradiance measurements were used to calculate the tilted irradiance at four different tilts; the results were then benchmarked with the reference cell measurements. During the conversion, all three loss mechanisms (temperature, spectral loss and reflectance loss) of a reference cell were accounted for.

From Table 1 it can be seen that the Perez model errors are well within the measurement uncertainties, which indicates a good performance of the model in a tropical environment (in this case Singapore).

The horizontal-to-tilt irradiance conversion uses two horizontal irradiance components to construct the tilted measurements following the Perez model. What is not shown above is that the diffuse components on the tilt can also be readily calculated. This leads to the following conversion method: two tilted reference cells are used to 'back calculate' the GHI; the modelled irradiance is then benchmarked using the GHI measurements obtained from the horizontally installed CMP11. This conversion is called the 'inverse Perez model'. Fig. 5 and Table 2 show the performance of the inverse Perez model, demonstrating that the modelling errors are smaller than the measurement uncertainty, and that the model can therefore be considered to be robust.

Conversion from tilt to horizontal using one reference cell

One question that might arise is why is it necessary to use measurements from two different tilts to reconstruct the GHI values? The answer is because the global-to-diffuse mapping is non-injective, i.e. it is a one-to-many mapping. In other words, for a particular GHI value, for example 800W/m^2, the corresponding DHI can have a varying range because of different meteorological conditions. Therefore, the use of one reference cell to reconstruct GHI and DHI simultaneously equates to solving for two unknowns using one equation [13]. Including another set of tilt measurements, however, provides an additional equation, which is then sufficient for solving for the two horizontal irradiance components.

Despite the mapping from GHI to DHI being non-injective, the irradiance conversion from tilt to horizontal is still possible by means of a decomposition model. A decomposition model separates DHI and HBI from GHI in situations when the DHI or HBI measurements are not available. Fig. 6 shows the first zero-energy house in Singapore: it has an 18.3°-tilted east-facing roof and a 6.1°-tilted west-facing roof, and reference cells are installed in each of the two corresponding POAs. An SPN1 sunshine pyranometer is installed horizontally at the ridge of the roof (sensors are not visible in the photograph). The application of the decomposition model is demonstrated using this set-up.

As the aim of this section is to reconstruct GHI using only one reference cell, the two reference cells (at different tilts) are used to separately reconstruct GHI. In the following experiment, the diffuse irradiance component obtained by SPN1 was assumed to be an unknown. The TGI measurements from the east-facing roof reference cell were decomposed into TBI and TDI by applying decomposition models (see Erbs, Klein, & Duffie [14], for example). The decomposed tilted irradiance components were then used to reconstruct GHI. A similar experiment was conducted using the west-facing reference cell alone. Table 3 shows the error terms in these two experiments.

It is concluded from Table 3 that the reference cell with smaller tilt produces better GHI estimates. It is also observed that the RMSE varies with the months owing to the fact that the decomposition model is very sensitive to sky conditions. Lastly, the errors of the tilt-to-horizontal conversion using only one reference cell are larger than those using two reference cells.

To analyse the results further, the converted GHI values are compared. In principle, if the conversion is accurate within an acceptable range, the GHI values obtained using the east-facing reference cell should be similar to those obtained using the west-facing reference cell. Fig. 7 shows a visual comparison of the converted GHI. In Fig. 7(a), GTI measurements on 2011 July 5 are plotted: it is clear that in the morning, the east-facing reference cell received more irradiance than the west-facing reference cell, whereas in the afternoon, the west-facing reference cell received more. In Fig. 7(b), it can be seen that the converted GHI values using the east-facing reference cell agree with the conversion results using the west-facing reference cell. Although the tilt-to-horizontal conversion errors when using a single reference cell are larger than those when using two reference cells, the conversion accuracies are still in the range of ~10% RMSE, which is acceptable for both PR calculations of PV systems without on-site readings and irradiance forecasting for power systems operation.

Tilted reference cells used	MBE [W/m^2]	RMSE [%]	U95 [%]
10° and 20°	–9.08	3.41	5.60
10° and 30°	–4.22	2.53	4.71
10° and 40°	–3.82	2.46	4.61
20° and 30°	10.59	3.66	5.66
20° and 40°	4.23	2.57	4.79
30° and 40°	–3.71	4.05	7.82

Table 2. Tilt-to-horizontal irradiance conversion errors using the 'inverse Perez model'. The calculated GHI values are compared with the pyranometer measurements. Mean bias error (MBE), root mean square error (RMSE) and the 95% expanded uncertainty (U95) are used as error metrics. All error terms include temperature, spectral loss and reflectance loss corrections.

Credit: Photo courtesy of Phoenix Solar Pte. Ltd.

Figure 6. The first zero-energy house in Singapore: the east-facing roof is tilted at 18.3° (right side of the roof), while the west-facing roof is tilted at 6.1° (left side of the roof).

Generating area-wide irradiance maps

Using the conversion technique described above it is now possible to combine readings from both horizontal pyranometers and reference cells in the POA, which helps in the creation of a denser network of sensors. To generate a fully spatially-resolved 2D irradiance map, a suitable interpolation algorithm needs to be developed. Conventional interpolation techniques – such as inverse distance-weighted interpolation, various types of kriging and optimal interpolation – have strengths and weaknesses in different circumstances.

Application of the spatio-temporal interpolation model developed by SERIS for the case of Singapore, using the readings from 25 stations for an area of ~700km^2, resulted in a fully interactive irradiance map for the country, shown in Fig. 8. The map displays the irradiance at any point within this area, either via cursor movements or by entering zip codes. When the 2D irradiance maps are referenced with actual measure-

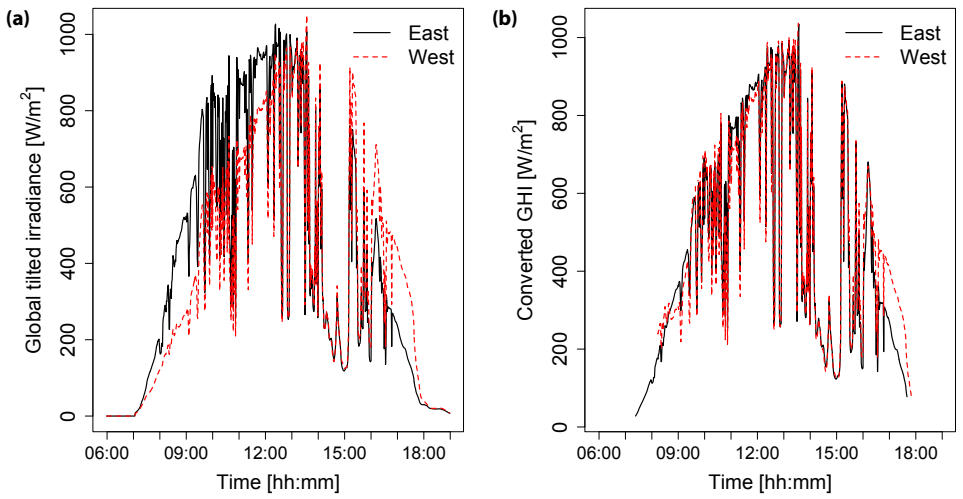

Figure 7. (a) Global tilted irradiance measurements on 5 July, 2011; (b) irradiance conversion from tilt to horizontal using only one reference cell. The converted GHI values using the east-facing and west-facing reference cells are in agreement.

Data	East MBE [W/m²]	East RMSE [%]	East U95 [%]	West MBE [W/m²]	West RMSE [%]	West U95 [%]
2011 Jan	–6.35	15.21	30.07	–1.87	9.65	18.96
2011 Feb	–15.66	12.00	24.40	–11.47	6.28	13.33
2011 Mar	–4.30	13.56	26.67	–4.78	9.29	28.39
2011 Apr	–9.14	12.80	25.44	–13.78	8.29	17.54
2011 May	–5.52	12.14	23.93	–12.90	8.10	17.16
2011 Jun	–5.18	13.45	26.51	–6.99	9.55	19.10

Table 3. Performance of the decomposition model of irradiance conversion from tilt to horizontal over a period of six months. TGI measurements from the individual reference cells are used as inputs; the outputs are benchmarked against the respective SPN1 GHI measurements. Mean bias error (MBE), root mean square error (RMSE) and the 95% expanded uncertainty (U95) are used as error metrics. All error terms include temperature, spectral loss and reflectance loss corrections. (Adapted from Yang et al. [13].)

ments from the 11 PV systems that were shown in Fig. 2, the uncertainties range from 6 to 31% for fine-time-resolution (<1 minute) irradiance interpolation, depending on the location and the spatial resolution. The higher values are naturally found in the outer areas of the island, where there are only one or two stations available for interpolation. This is less critical in larger countries, where the perimeter effect is less pronounced. The average uncertainty in the area with more sensors is 14%. This value can be significantly reduced through extending the sensor network, which would be possible by adding reference cell readings from existing – and future – PV installations and leveraging the conversion technique as described above.

Conclusion

Generating large-area irradiance maps would solve two challenges in today's PV industry: how to assess the performance of PV systems that do not have on-site irradiance measurement equipment installed, and creating a critical input for forecasting irradiance (and eventually the energy output of PV systems) in a spatially-resolved way for the grid operator to schedule the conventional power plants accordingly. Such irradiance maps require a dense network of irradiance sensors, which either is costly or does not necessarily provide the time or spatial resolution required (e.g. when using satellite data). Leveraging on the increasing number of PV systems that have irradiance measurement devices installed, typically in the plane of array, is therefore a cost-effective method for improving the accuracy of such forecasts. The technique described in this paper allows POA readings to be converted into GHI data, since the latter are required for a homogeneous, interpolated irradiance map. This has been successfully demonstrated in the case of Singapore. ■

Figure 8. An interactive tool developed by SERIS, showing a live irradiance map taken at 12:00 noon on 1 February, 2014. Locations of the 25 irradiance measuring stations (numbered 401–425) in Singapore are shown. (Map: Google Maps, retrieved 1 February, 2014.)

Authors

Dazhi Yang received his B.Eng. and M.Sc. from the National University of Singapore, where he is currently working towards a Ph.D. His research interests include statistical modelling for solar irradiance, forecasting methodologies and environmental data mining.

André Nobre received his M.Eng. in technology management from the University of South Australia. He is currently working towards a Dr.Eng. at the Universidade Federal de Santa Catarina in Brazil on short-term irradiance forecasting in tropical regions.

Rupesh Baker graduated with B.Eng. (mechanical engineering) from the National University of Singapore and has been involved in renewable energy consulting over the last three years. He is currently a PV systems engineer at SERIS.

Thomas Reindl received his Ph.D. from the University of Regensburg, Germany, and an MBA from INSEAD. He is currently the deputy CEO and cluster director of solar energy systems at SERIS. His research interests include high-efficiency PV systems and irradiance forecasting.

References

[1] Nobre, A. et al. 2012, "High performing PV systems for tropical regions – optimisation of systems performance", *Proc. 27th EU PVSEC*, Frankfurt, Germany.

[2] Dong, Z. et al. 2014, "Satellite image analysis and a hybrid ESSS/ANN model to forecast solar irradiance in the tropics", *Energy Conv. Man.*, Vol. 79, pp. 66–73.

[3] Yang, D. et al. 2013, "Block matching algorithms: Their applications and limitations in solar irradiance forecasting", *Energy Procedia*, Vol. 33, pp. 335–342.

[4] Gu, C. et al., "Spatial load forecasting with communication failure using time-forward kriging", *IEEE Trans. Power Syst.* [in press].

[5] Dong, Z. et al. 2013, "Short-term solar irradiance forecasting using exponential smoothing state space model", *Energy*, Vol. 55, pp. 1104–1113.

[6] Yang, D., Jirutitijaroen, P. & Walsh, W.M. 2012, "Hourly solar irradiance time series forecasting using cloud cover index", *Solar Energy*, Vol. 86, pp. 3531–3543.

[7] Yang, D. et al. 2013, "Solar irradiance forecasting using spatial-temporal covariance structures and time-forward kriging", *Renewable Energy*, Vol. 60, pp. 235–245.

[8] Yang, D. et al., "Solar irradiance forecasting using spatio-temporal empirical kriging and vector autoregressive models with parameter shrinkage", *Solar Energy* [in press].

[9] Meydbray, J., Emery, K. & Kurtz, S. 2012, "Pyranometers, reference cells: the difference", *pv magazine* (April).

[10] Ye, J. et al., "Determination of the PV module temperature coefficient from outdoor testing data" [submitted to Solar Energy].

[11] Perez, R. et al. 1987, "A new simplified version of the Perez diffuse irradiance model for tilted surfaces", *Solar Energy*, Vol. 39, pp. 221–231.

[12] Perez, R. et al. 1990, "Modeling daylight availability and irradiance components from direct and global irradiance", *Solar Energy*, Vol. 44, pp. 271–289.

[13] Yang, D. et al. 2013, "Evaluation of transposition and decomposition models for converting global solar irradiance from tilted surface to horizontal in tropical regions", *Solar Energy*, Vol. 97, pp. 369–387.

[14] Erbs, D.G., Klein, S.A. & Duffie, J.A. "Estimation of the diffuse radiation fraction for hourly, daily and monthly-average global radiation", *Solar Energy*, Vol. 28, pp. 293–302.